ACS MATERIALS LETTERS

www.acsmaterialsletters.org

Photoluminescent Humidity Sensors Based on Droplet-Enabled Porous Composite Gels

Yunyun Cheng,[†] Li Li,[†] Caleb H. Meredith, Rebecca V. Balaj, Dingbowen Wang, Meng Pan, Ting Han, Jian Yang, Qing Wang, Lijie Dong,* and Lauren D. Zarzar*

Cite This: *ACS Materials Lett.* 2023, 5, 2074–2083

Read Online

ACCESS | Metrics & More | Article Recommendations | Supporting Information

ABSTRACT: **Humidity sensors are important components in healthcare monitoring and advanced tactile sensing systems. However, low sensitivity and poor mechanical properties limit their practical applications in integrated haptic platforms such as artificial skin. Here, photoluminescence (PL)-type humidity sensing materials with simultaneously high sensitivity, stretchability, and healability are reported based on poly(vinyl alcohol) (PVA) composite gels comprising $Cd_xSe_{1-x}Zn_yS_{1-y}$ quantum dots (QDs). A droplet-assisted strategy is developed to achieve a uniform distribution of QDs throughout the polymer matrix and also to assist with, in combination with freeze−thaw and freeze−dry cycles, the formation of micropores during the gel preparation process that improves moisture adsorption. With further ligand optimization, the PVA/QD composite gels exhibit an excellent PL−humidity linearity (R^2 > 99%), a wide humidity sensing range (from 11% to 93%), short response/recovery time (~40 s), and good recoverability and cyclic stability (over 100 cycles). The humidity sensing mechanism is attributed to surface state changes of the QDs that are induced by intermolecular interactions between QD ligands and water molecules, as revealed by molecular vibration studies and density function theory calculations. This work opens avenues for the development of high-performance humidity-sensitive materials that are promising for next-generation tactile sensors and artificial skin and provides fundamental insights into the sensing mechanism of PL-based humidity QD sensors.**

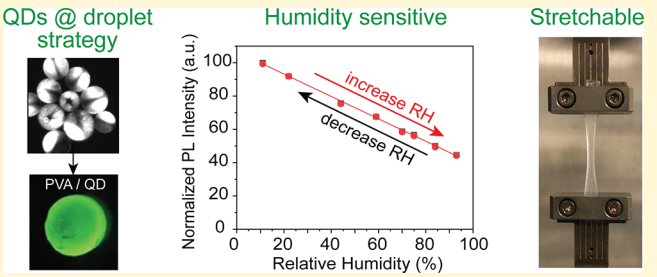

Humidity sensors are ubiquitously applied in a wide variety of modern industries, including agricultural planting, medical and health monitoring, and soft robotics.[1−5] In addition to a wide operating range, high sensitivity, and fast response/recovery time, humidity sensing materials for integrated and efficient haptic sensors and systems should possess flexibility, stretchability, and environmental stability. Although numerous humidity sensors based on inorganic materials such as ZnO,[6−8] CdS,[9] etc., have been developed, and they do show a wide sensing range and short response/recovery time, they are constructed either in bulk or thin films coated onto a rigid substrate and often suffer from poor flexibility and stretchability. Polymer composites that incorporate humidity-sensitive materials into more flexible materials, like poly(vinyl alcohol) (PVA), poly(dimethylsiloxane) (PDMS), etc., have also been extensively explored and are promising candidates for flexible humidity sensors due to their deformability, tailorability, and facile processing. Yet, a majority of polymer composite sensors still exhibit low moisture sensitivity, poor mechanical properties, and longer term environmental instability.[9−11] Further development of sensitive and reliable polymer composite materials is therefore important for humidity sensors.

Fundamentally, the working principle of most composite-based humidity sensors depends on electrical responses like changes in resistivity and capacitance,[2,4,9,10] which unfortunately can also be influenced by other external stimuli such as temperature and stress. Consequently, additional separators or electromagnetic shielding layers are often required to avoid electromagnetic interference, which undesirably increases the volume and weight of the devices. Recently developed photoluminescence (PL)-type optical humidity sensors based on luminescent materials embedded in a polymer matrix are a promising alternative that may enable efficient integration of multisensing functionalities into compact and lightweight sensor systems. In a typical PL-type composite humidity

Received: May 19, 2023
Accepted: June 27, 2023
Published: July 3, 2023

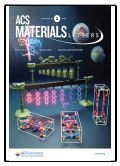

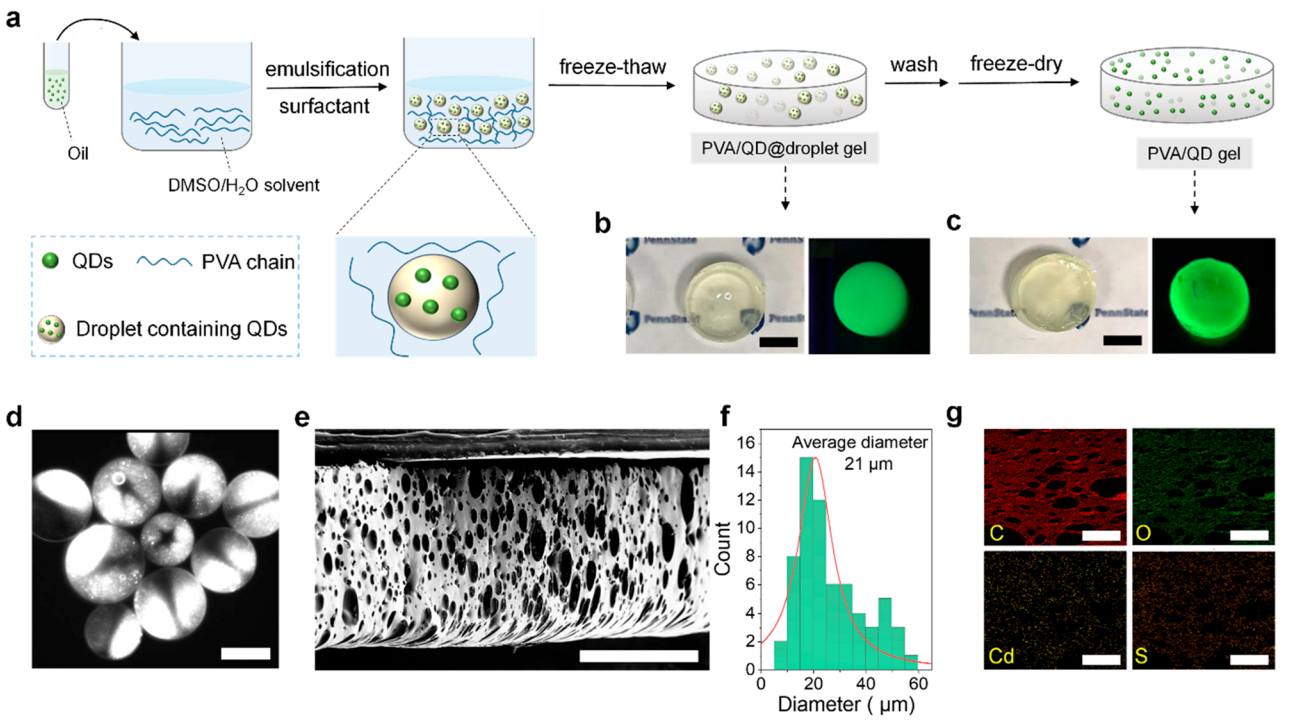

Figure 1. Gel preparation and characterization. (a) Schematic illustration of the fabrication procedures of a PVA/QD composite gel. (b) Optical image (left) and fluorescent image under UV 365 nm illumination (right) of the composite gel obtained after the freeze−thaw cycle. Scale bar: 1 cm. (c) Optical image (left) and fluorescence image (right) of the composite gel obtained after washing and freeze-drying. Scale bar: 1 cm. (d) Fluorescence micrograph of bromooctane-in-water droplets containing QDs stabilized by Triton X-100. The QDs are flowing inside the droplets due to Marangoni convection which creates the patterns observed within each droplet.[25] Scale bar: 20 μm. (e) Scanning electron micrograph of a PVA/QD composite gel. Scale bar: 100 μm. (f) Pore size (diameter) distribution of e. (g) Energy-dispersive X-ray mapping of a PVA/QD composite gel, including C, O, Cd, and S elements. Scale bar, 50 μm.

sensor, the humidity-sensitive parts are primarily fluorescent or phosphorescent organic molecules or quantum dots (QDs)[12−14] that exhibit humidity-induced PL quenching or an emission wavelength shift. In comparison to organic molecules, QDs have surface effects and quantum size effects that make them outstanding luminescent materials, exhibiting a tunable emission spectrum, narrow and symmetric emission peak, high photoluminescent quantum yield (PLQY), and long-term stability. Importantly, their luminescent properties are affected by surface chemical environments, e.g., ions, gases, *etc.*, and are easily tuned by surface ligands.[15−17] Therefore, QD-comprising polymer composites are promising for high-performance flexible humidity sensors and have been receiving increasing research interest.[12−14] For example, Xia et al. developed a PVA/SiO_2−CdTe QD composite film for a sensitive and stable humidity sensor with a wide sensing range of 5−97% RH.[18] Meng et al. reported a polystyrene-based fiber doped with CdSe/ZnS QDs that is flexible and sensitive to moisture with response/recovery times of 30/60 s in a range of 19−51% RH.[17]

Despite the progress achieved in polymer/QD composite-based humidity sensors, some critical challenges remain. Thus far, the QD ligands explored have mainly focused on water-soluble polar molecules like 3-mercaptopropionic acid (MPA) so as to enable dispersibility of QDs in water-rich solvents and improve the moisture sensitivity of the resultant polymer/QD composite.[18,19] However, such functionalized QDs usually suffer from significantly reduced PLQYs due to weak QD-ligand interactions and thus less passivated surfaces defects (such as dangling bonds),[16,20] which in turn hamper the humidity sensing efficiency and increase the cost. For example, the PLQY of CdSe/CdS/ZnS QDs modified with a hydrophilic polyoxyethylene octadecylamine (PEGO) ligand decreases from 78% to 47%.[20] Second, the QD-polymer composites usually suffer from a high sensing hysteresis, i.e., long response/recovery time, due to slow moisture adsorption and diffusion in the polymer matrix. Although porous structures have been constructed in the polymer to improve the adsorption efficiency of water molecules, they are usually made at the cost of reduced mechanical strength, toughness, and stability,[19,21] which is not desired for the long-term operation of a humidity sensor. For instance, microsized pores were achieved in a PVA film via electrospinning yielded films with a limited tensile strength of ∼5 MPa and a maximum strain of ∼500% with poor structural integrity in humid environments.[19] Therefore, it is still important and challenging to design and fabricate humidity sensors that are highly sensitive, quickly responsive, and mechanically robust for high-performance humidity sensors.

Herein, we report a PVA/QD composite gel-based PL-type humidity sensor with high sensitivity and stability, short response-recovery time, and high toughness by utilizing a facile "droplet-assisted" strategy combined with ligand optimization. We show that oil-in-water emulsion droplets, serving as a medium, encapsulate hydrophobically functionalized QDs in the aqueous solution and lead to simultaneously a uniform dispersion of QDs and pore structures within the PVA matrix, which is beneficial for moisture adsorption and toughness enhancement. Several QD ligands (oleic acid, 3-mercaptopropionic acid, and 3-aminopropanol) with different chemical

https://doi.org/10.1021/acsmaterialslett.3c00529
ACS Materials Lett. 2023, 5, 2074−2083

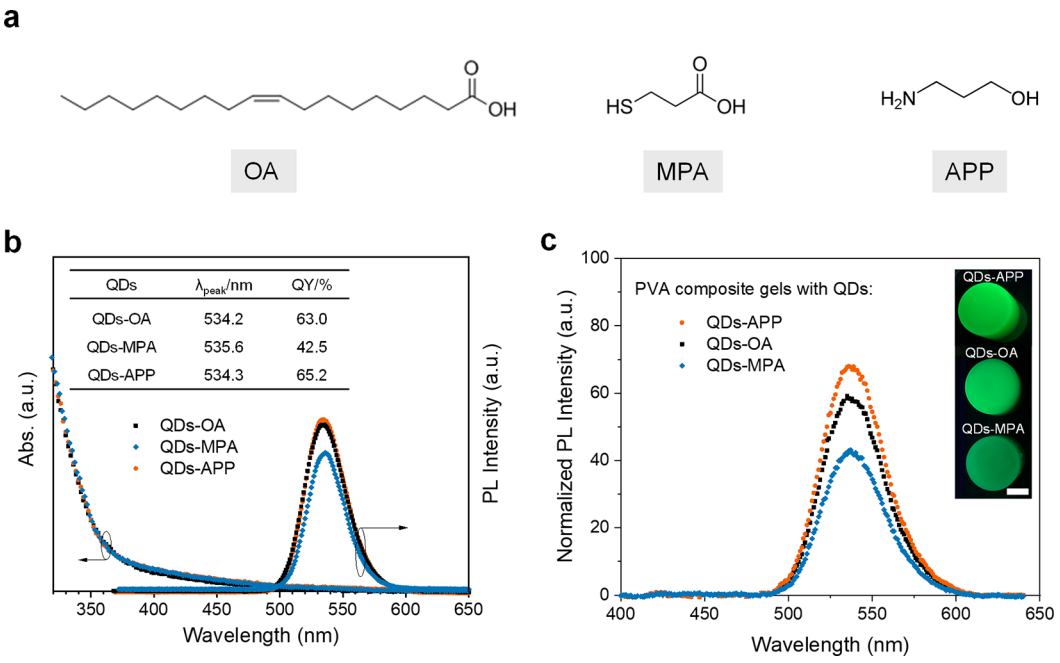

Figure 2. Influence of the QD ligand on gel PL. (a) Chemical structures of QD ligands: OA, MPA, and APP. (b) UV−vis absorption and PL emission spectra (excited at 350 nm) of QDs with different ligands dispersed in chloroform (for QDs-OA and QDs-APP) or water (for QDs-MPA). (c) Normalized PL spectra of PVA composite gels with QDs with different ligands. Inset are fluorescent images of PVA composite gels with different QDs. Scale bar, 1 cm.

structures are compared, and we confirm the significant role of the ligand on tuning the photoluminescent and humidity sensing properties of the PVA/QD composite gels. Molecular spectroscopy and density functional theory (DFT) calculations are used to study the effects of QD surface state changes induced by intermolecular interactions and electron transfer between ligands and water molecules on the humidity sensing mechanism. The resultant PVA/QD composite gels exhibit excellent humidity sensing performance with a short response/recovery time of ∼40 s in 11−93% RH, stability over 100 cycles, enhanced mechanical toughness (∼2850% strain and ∼300 MJ/m^3), and self-healing capabilities which make this composite promising for applications in next-generation tactile sensing systems and health monitoring.

PVA was chosen as the polymer matrix due to its favorable hydrophilic properties, ease of processability, and low cost. $Cd_xSe_{1-x}Zn_yS_{1-y}$ QDs were selected as the primary humidity-responsive component in the composite gels owing to their high PLQYs, high sensitivity of moisture, monodispersity, and high chemical stability compared to other QDs such as carbon QDs, CdTe QDs, *etc.*[15,16] The QDs were prepared by a single-step synthesis method described in the experimental methods of the Supporting Information.[16] The QD composition and size (diameter ∼7.6 ± 0.8 nm) were confirmed by transmission microscopy (TEM) and energy dispersive X-ray spectroscopy (EDS) mapping (Figures S1 and S2), in accordance with our previous work.[22,23] The surface structure of as-synthesized QDs modified by oleic acid (OA) ligand was confirmed by Fourier-transform infrared (FT-IR) absorption spectra (Figure S3, Supporting Information). The PVA/QD composite gel was then prepared by using our devised "droplet-assisted" method followed by freeze−thaw and freeze−dry procedures, as schematized in Figure 1 and described in detail in the Supporting Information. In brief, QDs were first dispersed in a nonpolar oil, e.g., bromooctane, bromohexane, octane, *etc.*, with a concentration of 1 mg/mL. Meanwhile, 15 wt % of PVA was fully dissolved in a dimethyl sulfoxide (DMSO)/H_2O binary solvent (4:1 v/v) at 120 °C for 2 h. We found that using DMSO endows the PVA gels with much higher mechanical strength and toughness in comparison to the gels prepared by using only water (Figures S4 and S5) due to more tightly packed polymer chains (thus higher crystallinity) and improved hydrogen bonding interactions.[24] Upon cooling to 60 °C and vigorously stirring, 1 mL of QD-oil solution was then emulsified by vortex mixing with 5 mL of the as-prepared PVA solution with the help of added surfactant, e.g., 0.1 to 0.2 wt % Tergitol NP-9, sodium dodecyl sulfate (SDS), or Triton X-100. After one freeze−thaw cycle followed by washing in water (to remove the DMSO and surfactant) and freeze-drying, the green-fluorescent PVA/QD composite gel was obtained (Figure 1b, c and Figure S6 and S7). The fluorescence micrographs of the precursor emulsion (Figure 1d and Video S1) showed a uniform distribution of QDs inside the droplets with an average droplet diameter of 28 ± 5 μm (Figure S8). The scanning electron micrograph (SEM) image of the composite gel (Figure 1e) revealed an average pore diameter of 21 ± 3 μm (Figure 1f), where the pores were templated by the oil droplets embedded inside the PVA along with some degree of volume shrinkage occurring during the freeze-drying process. Energy dispersive X-ray spectroscopy (EDS) elemental mapping of the dry composite (Figure 1g) revealed a homogeneous distribution of Cd and S elements from the QDs, signifying a uniform dispersion of QDs throughout the PVA matrix. Additionally, we did not observe Br or Na elements in the EDS survey (Figure S9), indicating that most of the brominated oil and surfactant (in the case of SDS) were removed during washing.

After fabrication, we carefully investigated the photoluminescence properties of the composite gels. We expected that the oil, surfactant, and QD ligands may potentially affect

https://doi.org/10.1021/acsmaterialslett.3c00529
ACS Materials Lett. 2023, 5, 2074−2083

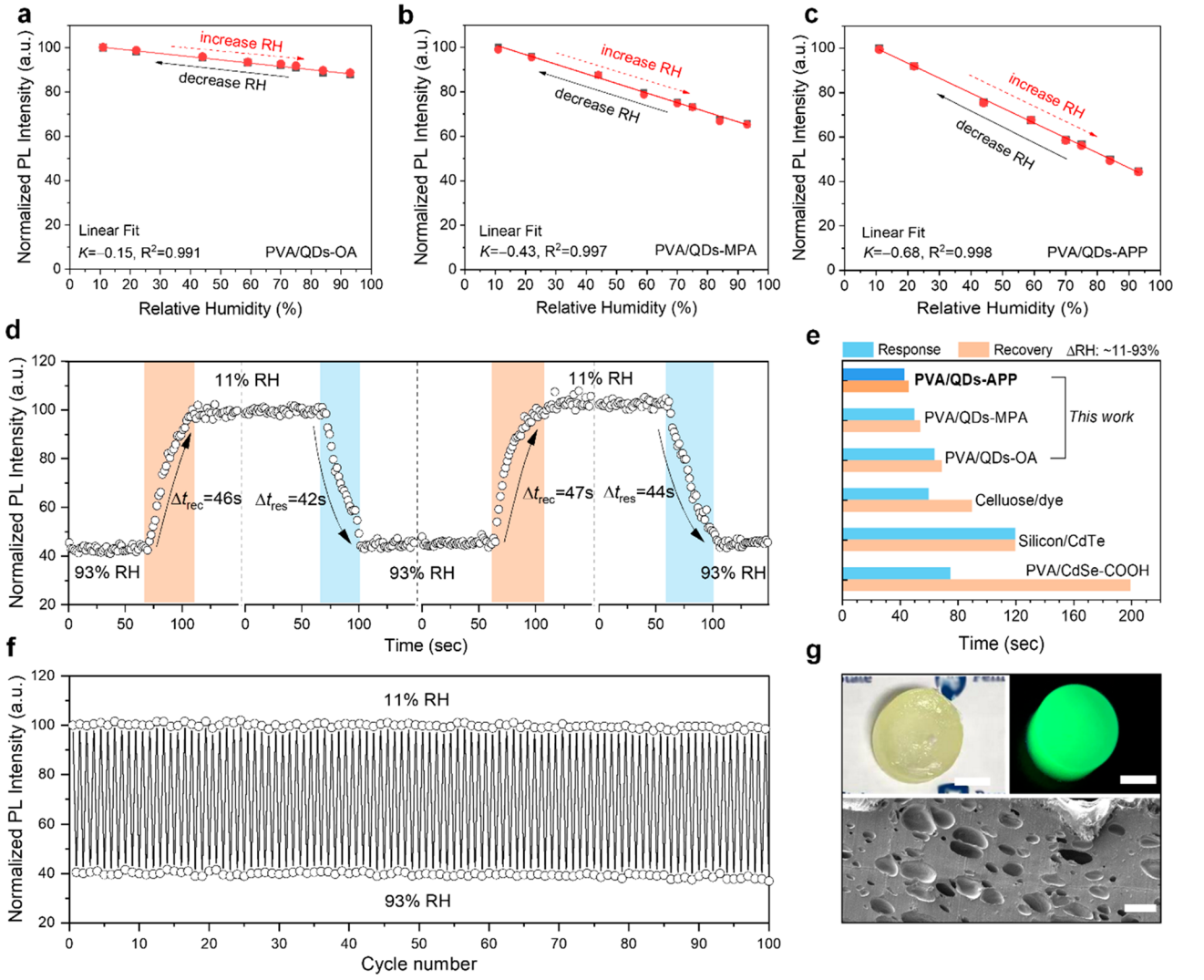

Figure 3. Normalized PL intensity as a function of RH from 11% to 93% (red dot) and 93% to 11% (black dot) of (a) PVA/QDs-OA, (b) PVA/QDs-MPA, and (c) PVA/QDs-APP composite gels. Red lines are the linear fit to the experimental data. (d) Time-dependent PL intensity of the PVA/QDs-APP composite gel when RH changes between 11% and 93%. (e) Comparison of response and recovery time between this work and other typical optical humidity sensors in literature.[17−19,27−35] (f) Cyclic stability of the PVA/QDs-APP composite gel under alternatively changed RH between 11% and 93%. (g) Photograph (upper left), fluorescence photograph (upper right), and SEM image (lower) of the gel after 100 cycles, with scale bars of 1 cm, 1 cm, and 20 μm, respectively.

the photoluminescent properties of the gels. We picked three common oils, i.e., bromooctane, bromohexane, and octane (Figure S10), which are cost-effective and widely used for emulsions, to prepare the PVA/QD composite gels. We found that QDs can be well-dispersed in all these oils, and bright luminescence is observed in the resultant PVA/QD composite gels, indicating that the influence of oils was negligible (Figure S10). To study the effects of added surfactants, we examined three commonly used surfactants, Triton X-100, SDS, and Tergitol NP-9. SDS is anionic while Triton X-100 and Tergitol NP-9 are nonionic (Figure S11). The PL spectra and recorded fluorescent images of the gels demonstrate that all of these surfactants can help to improve the stability and dispersion of QD-containing droplets in the PVA gel, leading to comparably high PL intensity. We believe that the oil and surfactant act as a "medium" to produce and stabilize QD-containing droplets dispersed within the PVA matrix during gel preparation but which after subsequent washing steps appear to have little influence on the photoluminescent properties of the gels.

We next explored the influence of the QD ligand on the photoluminescence properties of the composite gels. Three typical organic ligands were chosen to modify the surface of QDs, i.e., oleic acid (OA), 3-mercaptopropionic acid (MPA), and 3-aminopropanol (APP) (Figure 2a). The long-chain OA is one of the most commonly used nonpolar QD ligands and renders the QDs hydrophobic, while MPA and APP are short and polar, endowing the QDs with better moisture affinity. When the QDs were initially synthesized, they were functionalized already with the OA ligand through the coordination interactions between metal ions (M^{2+}, i.e., Cd^{2+}, Zn^{2+}) in the QDs and −COOH group in OA. The MPA and APP ligands were grafted to the QD surface by $M^{2+}\cdots$SH− and $M^{2+}\cdots$NH− interactions, respectively, through a ligand exchange method as described in our previous work.[22,23,26] The corresponding QDs modified by OA, MPA and APP were denoted as QDs-OA, QDs-MPA and QDs-APP, respectively. The different ligand-modified surface structures of QDs were confirmed by FT-IR absorption spectroscopy (Figure S3). The PL spectra and

https://doi.org/10.1021/acsmaterialslett.3c00529
ACS Materials Lett. 2023, 5, 2074−2083

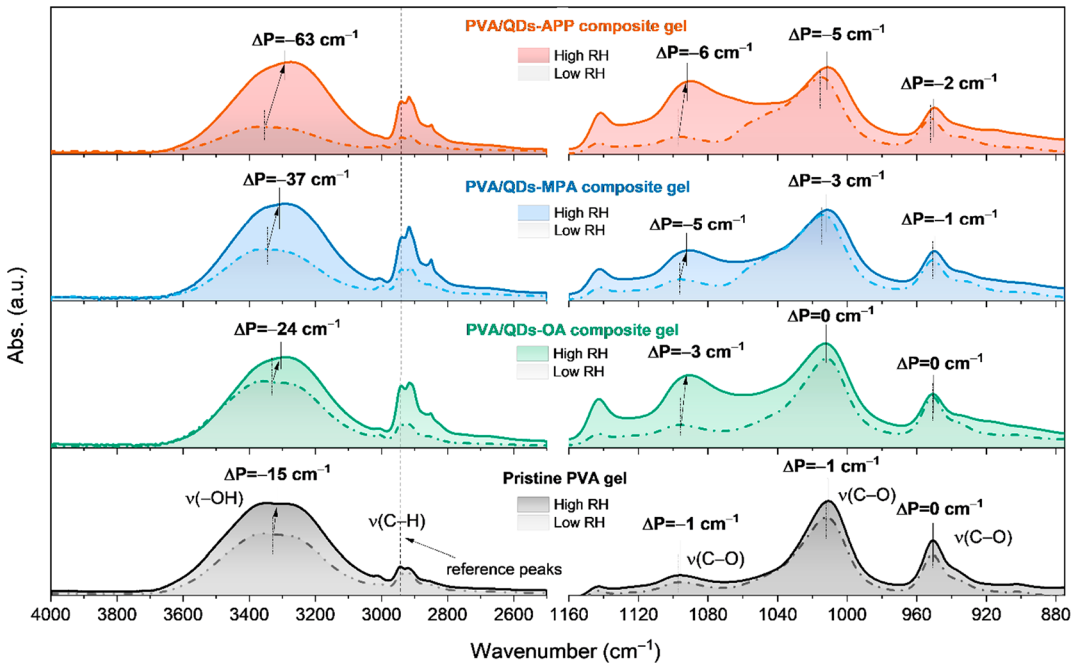

Figure 4. FTIR-ATR absorbance spectra of pristine PVA gel and the various composite gels under low RH (20%, dashed-dotted line) and high RH (90%, solid line). The black arrows indicate the peak shift between high and low RH conditions.

PLQY measurements of the various QDs are presented in Figure 2b. The QDs-OA show a PLQY of ∼60.5%, while weaker PL intensity and a lower PLQY (43.6%) were observed in QDs-MPA. Such decrements have been widely reported and well understood by the fact that the weak $M^{2+}\cdots SH-$ coordination interactions between MPA and QDs leads to inadequate surface defect passivation and extra trap levels.[15,16,22] Comparatively, QDs-APP exhibited the highest PL intensity with a PLQY of 62.1%, which is attributed to the strong $M^{2+}\cdots NH-$ interactions and thus efficient defect passivation.

The photoluminescent properties of the resultant PVA composite gels prepared with QDs-OA, QDs-MPA and QDs-APP were then measured (Figure 2c). The gels comprising QDs-OA and QDs-MPA exhibited significantly lower PL intensity compared with the PVA/QDs-APP gel. Variations in PL intensity are also possibly related to differences in the dispersions of QDs in the PVA matrix, wherein aggregation can cause PL quenching. Fluorescence optical micrographs of the gels revealed that the gels with QDs-OA and QDs-MPA display larger bright spots especially when wet, compared to gels with QDs-APP, suggesting that QD aggregates may lead to quenching (Figure S12). To better reveal the nanoscale dispersity of QDs in the gels, we took TEM images of ∼50 nm thick gel slices, (Figure S13). The QDs-APP showed a relatively homogeneous distribution in the PVA matrix with an average particle cluster diameter (d) of 10∼20 nm, while QDs-OA and QDs-MPA were aggregated with d values of ∼50 and ∼100 nm, respectively. The aggregation of QDs can lead to undesired charge transfer between QDs and thus exciton recombination loss, resulting in the decreased PL intensity in the composite gels. Therefore, QDs-APP, which has the best dispersibility, also exhibits the strongest photoluminescence. Hence, in contrast to the negligible effect of the oils and surfactants tested, variation in the surface ligands of the QDs had a significant impact on the photoluminescent properties of the PVA/QD composite gels.

We next studied the PL intensity-based humidity sensing properties of the various PVA/QD composite gels (Figure 3 and Figures S14−S16). A series of relative humidity environments (RH, from 11% to 93%) were made using saturated salt solutions in a sealed chamber connected to the fluorescence spectrograph. The humidity was calibrated with a commercial humidity sensor. From Figure 3a−c, we see that the PL intensity for all three composite gels dropped as the humidity increased from 11% RH to 93% RH, showing a linear PL response with a fitting factor $R^2 > 99\%$. All gels also had good recoverability over a wide humidity range. However, the humidity sensitivity, defined as the slope (K) of the linear fit to the PL−RH data, varied significantly between the gels; i.e., K is −0.14, − 0.43, and −0.68 for the composite gels with QDs-OA, QDs-MPA and QDs-APP, respectively. Higher absolute values of K represent higher humidity sensitivity. Compared with the hydrophobic OA ligand, the more polar MPA and APP ligands exhibited higher humidity sensitivity, possibly due to the polar interactions with water molecules. The mechanism will be discussed in detail later.

A desirable humidity sensor requires not only high sensitivity but also short response and recovery times to alleviate sensing hysteresis. Figure 3d shows the time-dependent PL intensity for the PVA/QDs-APP gel, which was realized by collecting the maximum PL intensity (i.e., at ∼530 nm) under continuous UV excitation at 350 nm as the humidity was alternatively changed between high RH (∼93%) and low RH (∼11%). The average response and recovery time from over 5 cycles was 43 ± 3 s and 46 ± 4 s, respectively. Using the same method, the response/recovery time of PVA/QDs-MPA and PVA/QDs-OA gels was also determined, i.e., 56/64 s and 94/109 s, respectively, as presented in Figure 3e. Notably, the response/recovery time of PVA/QD-APP gel was not only the shortest among the three gels but also outperforms most reported optical humidity sensors, even those of resistive-/capacitive-type in the literature (Figure 3e and Table S1).[17−19,27−35] For example, the response/recovery

https://doi.org/10.1021/acsmaterialslett.3c00529
ACS Materials Lett. 2023, 5, 2074−2083

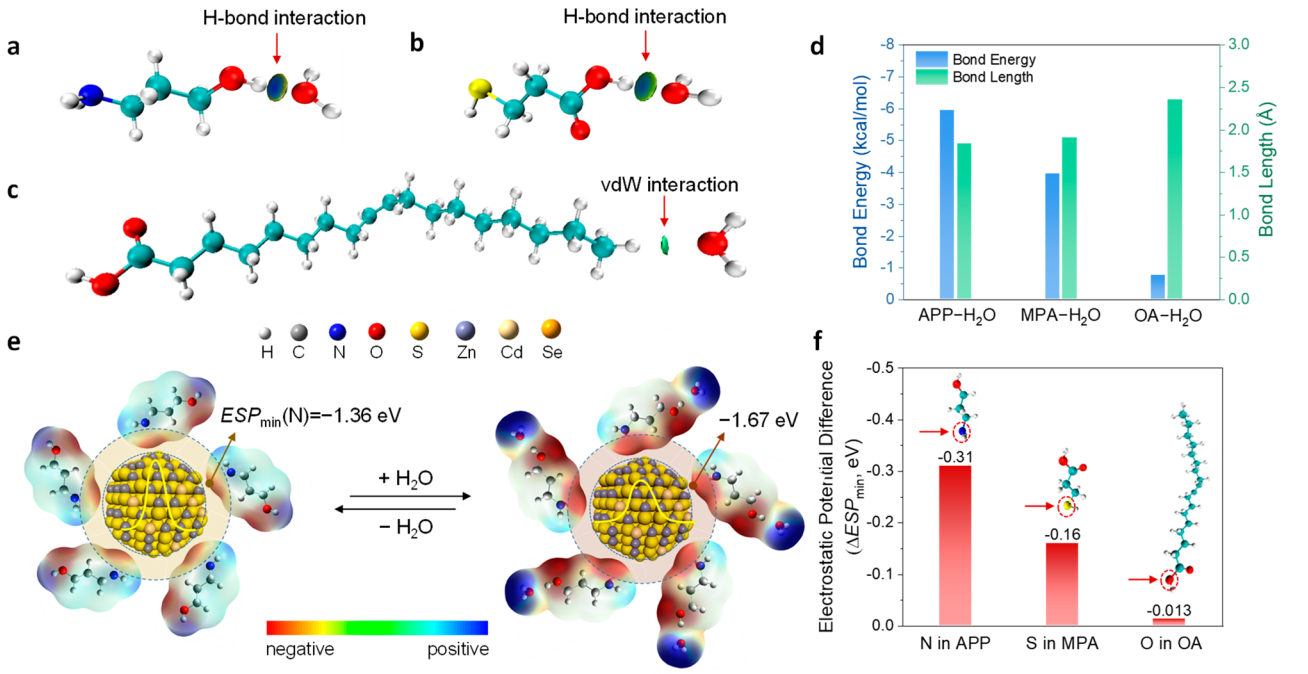

Figure 5. DFT calculations. Visualizations of intermolecular interactions based on IGMH analyses of (a) APP−H_2O, (b) MPA−H_2O, and (c) OA−H_2O complexes. (d) Calculated bond energies and bond lengths of hydrogen bonds in APP-H_2O and MPA-H_2O complexes and vdW interaction in the OA−H_2O complex. (e) Electrostatic potentials of APP (left) and APP−H_2O (right) outside QDs, with the calculated electrostatic potential minima of the N atom annotated. The ligands and ligand-water complexes around the QDs were drawn schematically and were not specifically modeled. (f) Gained electrostatic potential differences of N (in APP), S (in MPA), and O (in OA) atoms at the surface of QDs after adsorbing water molecules.

time of a porous silicon/CdTe-MPA composite is 120/120 s (5∼56% RH).[35] Considering that the gel thickness may be a potential factor affecting the humidity sensing properties, we also investigated the relationship between gel thickness (1 to 20 mm range) and humidity sensitivity/recovery time (Figures S17 and S18). As may be expected, the results demonstrate that the humidity sensitivity (which is an equilibrium property) demonstrates no significant variation with the sample thicknesses. However, the recovery time is inversely correlated with thickness, since it takes more time for water molecules to diffuse across a thicker sample. However, while the thickness should be as thin as possible to generate the fastest response, there is a trade-off with mechanical strength, which we found decreased for thin samples (Figure S19). In general, the samples used in this work are ∼5 mm thick.

Another important factor for a humidity sensor is cyclic reliability, which describes the reproducibility of the response as the humidity is changed. We collected the maximum PL intensity of the PVA/QDs-APP composite gel over 100 cycles, where 1 cycle means RH changes from 11% to 93% to 11%. As shown in Figure 3f, no apparent deviations of PL intensity were observed during cycling, demonstrating the excellent cyclic stability of the composite gel. After 100 cycles, the gel exhibited no noticeable deformation in shape and still exhibited bright fluorescence with intact inner pore structures (Figure 3g).

To investigate the humidity sensing mechanism, we collected and compared the Fourier-transform infrared (FT-IR) spectra of pure PVA gel and the various PVA/QD composite gels under low (∼20%) and high (∼90%) RH environments (Figure 4). All gels were prepared under the same conditions (DMSO/H_2O binary solvent, bromooctane oil droplets, and Triton X-100 surfactant). The broadest peaks at 3600−3000 cm^{-1} are attributed to the vibration of the −OH group, and the three other peaks at 1100, 1016, and 950 cm^{-1} correspond to the vibrations of C−O group.[36] We see that after the humidity changes from low RH to high RH, the broadest peaks (−OH group) shift to lower wavenumbers (i.e., red shift) in all four gels, signifying that hydrogen bonds are formed between water molecules and the gels. Compared with pure PVA, where a 15 cm^{-1} red shift was observed, the PVA/QD composite gels exhibited much larger shifts, i.e., 24 cm^{-1}, 37 cm^{-1}, and 63 cm^{-1} for PVA/QDs-OA, PVA/QDs-MPA, and PVA/QDs-APP composite gels, respectively. Similar results were also observed for the other three peaks. As a reference, the peaks at around 2940 cm^{-1} that correspond to the vibration of the C−H group do not show position shifts in the gels regardless of the RH. It is thus derived that the ligand-water interactions are different among these gels, which may be the reason behind such varied humidity sensing properties.

To gain a deeper understanding of the mechanism leading to the IR peak shifts and the humidity-sensing mechanism, we conducted DFT calculations on the three QD systems. We first examined the intermolecular interactions between the ligands and water molecules after geometry optimizations at a b3LYP/6-311g** level within Gaussian,[37] as depicted in Figure S20 and S21. As expected, hydrogen bonds (H−bonds) are formed in APP−H_2O and MPA−H_2O complexes, while only weak van der Waals (vdW) interactions exist between the OA ligand and water molecules. We consider only the water-alkyl interactions in the OA-H_2O complex; this is because the carboxyl group on the OA ligand coordinates to the QDs, and the water is unlikely to diffuse through the hydrophobic, long alkyl chain of the OA to reach the QD surface. The independent gradient model based on Hirshfeld partition (IGHM) was further used to directly visualize the interaction differences between the

https://doi.org/10.1021/acsmaterialslett.3c00529
ACS Materials Lett. 2023, 5, 2074−2083

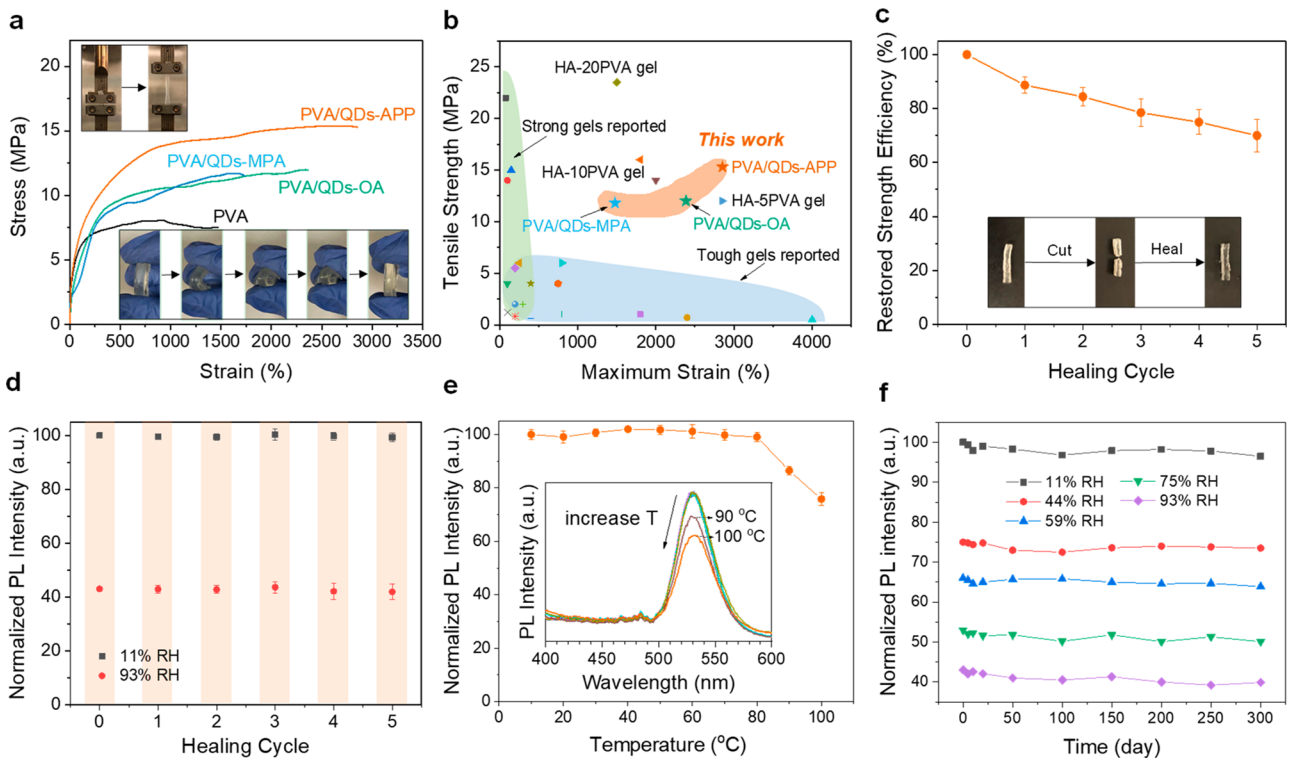

Figure 6. Mechanical properties, thermal stability, and self-healing ability of the composite gels and effects on humidity sensing. (a) Stress−strain curves of pristine PVA gel and various PVA-based composite gels, insets show photographs of tensile (top) and bending (bottom) tests. (b) Comparison of tensile strength and maximum strain between this work and other reported work.[44−48] The HA-20PVA, HA-10PVA, and HA-5PVA gels are hydrated with a water content of ∼70%, ∼76%, and ∼88%, respectively. (c) Restored mechanical strength efficiency of the PVA/QDs-APP composite gel during 5 cutting-healing cycles. Insets are the optical images of the PVA/QDs-APP composite gel during one cutting-healing cycle. (d) Normalized PL intensity of the PVA/QDs-APP composite gel at 11% RH (black dot) and 93% RH (red dot) during 5 cutting-healing cycles. (e) Normalized PL intensity of the PVA/QDs-APP composite gel as temperature changes from 10 to 90 °C. Inset shows the PL spectra of the gel collected at different temperatures. (f) Normalized PL intensity of the PVA/QDs-APP composite gel at various RHs over 300 days.

ligand−water complexes,[38,39] as shown in Figure 5a−c. The intermolecular interactions can be visually distinguished by the isosurfaces between two molecules with different colors, i.e., blue, green, and red represent attractive interaction, weak intermolecular interaction, and repulsive interaction, respectively. Isosurfaces between APP and H_2O, and between MPA and H_2O, are represented by dark blue ellipsoids, while a small green isosurface is shown in the OA−H_2O complex, verifying the relatively strong hydrogen bonding interactions in APP−H_2O and MPA−H_2O complexes in comparison to the weak vdW interactions between the OA ligand and water. Quantitatively, the interaction energy calculations, after basis set superposition error (BSSE) correction, show that the bonding energy is −5.95, −3.90, and −0.76 kcal/mol for APP−H_2O, MPA−H_2O and OA−H_2O, respectively, and the corresponding bond lengths are 1.836, 1.904, and 2.360 Å, respectively (Figure 5d) indicating that the APP−H_2O complex has the strongest interactions. Moreover, we find that the O−H bond near the H−bond becomes stretched after the H−bond formation; e.g., the bond length is increased from 0.974 to 0.982 Å in APP and from 0.969 to 0.972 Å in MPA. It is well understood that the stretched bonds have a weaker force constant and would lead to a reduced vibration frequency in accordance with the IR results.

We further examined by DFT calculations the electrostatic potential (ESP) distributions of the ligands when adsorbing and desorbing water molecules (Figure 5e and Figures S23 and S24). Results showed that the ESP of the ligands changes significantly due to the formation of H-bonds. Electron transfer occurs along the H-bond from the water molecule to the ligand, leading to increased negative potentials at the O atom adjacent to the H-bond. Moreover, the other end of the ligand (−NH_2 group) also receives increased negative potential, e.g., the ESP minimum of N [ESP_{min} (N)] in APP is changed from −1.36 to −1.67 eV. Considering this site (−NH_2) is where the ligands coordinately bind with the surface atoms (Cd or Zn) of QDs, the formation of H−bonds therefore changes the coordination balance between the QDs and ligands. The additionally accumulated negative potential (ΔESP) at the surface of the QDs would then compress the electron wave function and introduce extra surface defect states, which reduces the probability of electron−hole recombination and finally results in lower PL intensity, as described by the PL quenching mechanism.[40,41] Since the process is physically reversible, the surface states and thus luminescent properties of QDs can be restored after water molecules desorb. Such mechanisms are similar to previous reports on gas sensing, e.g., the adsorption of negatively charged SCN^- or OH radicals onto the surface of QDs can lead to PL quenching.[42,43] ΔESP_{min} is calculated to be −0.31, − 0.16 and −0.013 eV for N in APP, S in MPA and O in OA, respectively (Figure 5f), indicating that the moisture-induced PL quenching follows the trend of QDs-APP > QDs-MPA > QDs-OA, which is in agreement with the experimental observations.

https://doi.org/10.1021/acsmaterialslett.3c00529
ACS Materials Lett. 2023, 5, 2074−2083

In addition to the excellent humidity sensing properties, we found that the composite gels also exhibit enhanced mechanical properties, good temperature stability, and a self-healing ability. As presented in Figure 6a, the composite gels showed a higher tensile strength and toughness than pure PVA gel. The PVA/QD-APP composite gel exhibited a high strength of ∼15 MPa and a maximum strain of ∼2850%, which are 1.88 and 1.93 times those of pure PVA gel, respectively. The PVA/QDs-APP composite gel, with both high strength and toughness (∼300 MJ/m^3), is on par with the best reported polymeric gels that are either mechanically strong or tough (Figure 6b).[44−48] The favorable mechanical properties may enable the gel sensor to withstand harsh mechanical conditions (e.g., stress, or deformation). We attribute the improved mechanical properties of the PVA/QD gels to enhanced crystallinity (Figure S25) and nanofiller-induced mechanical reinforcement effects that originate from the ultrasmall QDs in the PVA matrix, as supported by previous reports.[49,50] As shown in Figure 6c, after mechanical damage (such as cutting), the composite gel can undergo a self-healing process upon wetting and contacting the fractured sections for 2 h at 60 °C, owing to the dynamic hydrogen bonding network of PVA, similar to previous work.[51,52] The tensile strength can be restored to ∼70% of the original value after 5 cutting-healing cycles. Owing to the fact that the PL responses stem from the QDs inside PVA, the humidity sensing functionality of the composite gels is barely affected by mechanical damage, as seen in Figure 6d. We further examined the temperature stability of the composite gel-based humidity sensor (Figure 6e). The PL emission is unaffected until the temperature reaches ∼80 °C, above which irreversible PL quenching occurs due to thermally activated carrier traps.[16,19,41] Little deterioration in the gel PL intensity was found over 300 days (Figure 6f). These results suggest that the PVA/QDs-APP composite gel is a reliable humidity sensor that can be potentially applied to various scenarios.

In conclusion, we have reported PL-type, PVA/QD composite humidity sensing gels with high sensitivity, stretchability, and healability. The use of the APP ligand for QDs significantly enhances the photoluminescence properties and humidity sensitivity of the composite gels. The developed strategy of using emulsion droplets during the gel fabrication leads to not only porous structures that improve moisture adsorption but also contributes to a more uniform distribution of QDs throughout the polymer matrix. The PVA/QDs-APP composite gel exhibits high humidity sensitivity and a fast response/recovery rate that are comparable to or better than those of many state-of-the-art humidity sensing optical and electronic materials. The humidity sensing mechanism is attributed to surface state changes of the QDs that are induced by polar interactions between the ligands and water molecules. The enabling properties of stretchability due to high mechanical toughness, healability arising from dynamic hydrogen bonds, and excellent stability make the gels tolerant to various environments. This work opens up a route to high-performance stretchable humidity sensors that are promising for applications and provides fundamental insights into the sensing mechanism of PL-based humidity QD sensors.

■ ASSOCIATED CONTENT

Data Availability Statement

The data that support the findings of this study are available in the Supporting Information of this article.

Supporting Information

The Supporting Information is available free of charge at https://pubs.acs.org/doi/10.1021/acsmaterialslett.3c00529.

Experimental section, characterizations, TEM images of QDs, FTIR spectra of QDs, optical images of gels, stress−strain curves of gels, fluorescent microscopic graphs of QD-oil emulsions, EDS spectra of gels, chemical structure of oils and PL spectra of QDs, chemical structure of surfactants, fluorescent microscopic graphs of gels, TEM images of gels, PL spectra of gels at varied RHs, PL intensity as a function of RH, recovery time as a function of gel thickness, tensile strength as a function of gel thickness, ball−stick models of chemical structure of QDs with different ligands, electrostatic potentials of QD ligands, DSC curves of gels, and comparison of humidity sensing properties (PDF)

Video S1, oil-in-water droplets containing QDs (MP4)

■ AUTHOR INFORMATION

Corresponding Authors

Lijie Dong − *Center for Smart Materials and Devices, State Key Laboratory of Advanced Technology for Materials Synthesis and Processing, Wuhan University of Technology, Wuhan, Hubei 430070, P. R. China;* orcid.org/0000-0002-6919-9498; Email: dong@whut.edu.cn

Lauren D. Zarzar − *Department of Chemistry and Department of Materials Science and Engineering, The Pennsylvania State University, University Park, Pennsylvania 16802, United States;* orcid.org/0000-0002-3287-3602; Email: ldz4@psu.edu

Authors

Yunyun Cheng − *Center for Smart Materials and Devices, State Key Laboratory of Advanced Technology for Materials Synthesis and Processing, Wuhan University of Technology, Wuhan, Hubei 430070, P. R. China; Department of Chemistry, The Pennsylvania State University, University Park, Pennsylvania 16802, United States*

Li Li − *Center for Smart Materials and Devices, State Key Laboratory of Advanced Technology for Materials Synthesis and Processing, Wuhan University of Technology, Wuhan, Hubei 430070, P. R. China; Department of Materials Science and Engineering, The Pennsylvania State University, University Park, Pennsylvania 16802, United States*

Caleb H. Meredith − *Department of Materials Science and Engineering, The Pennsylvania State University, University Park, Pennsylvania 16802, United States*

Rebecca V. Balaj − *Department of Chemistry, The Pennsylvania State University, University Park, Pennsylvania 16802, United States*

Dingbowen Wang − *Department of Biomedical Engineering, Materials Research Institute, The Huck Institutes of the Life Sciences, The Pennsylvania State University, University Park, Pennsylvania 16802, United States;* orcid.org/0000-0003-4034-2024

Meng Pan − *Center for Smart Materials and Devices, State Key Laboratory of Advanced Technology for Materials Synthesis and Processing, Wuhan University of Technology, Wuhan, Hubei 430070, P. R. China*

Ting Han − *Center for Smart Materials and Devices, State Key Laboratory of Advanced Technology for Materials Synthesis*

https://doi.org/10.1021/acsmaterialslett.3c00529
ACS Materials Lett. 2023, 5, 2074−2083

and Processing, Wuhan University of Technology, Wuhan, Hubei 430070, P. R. China

Jian Yang − *Department of Biomedical Engineering, Materials Research Institute, The Huck Institutes of the Life Sciences, The Pennsylvania State University, University Park, Pennsylvania 16802, United States;* orcid.org/0000-0003-0695-828X

Qing Wang − *Department of Materials Science and Engineering, The Pennsylvania State University, University Park, Pennsylvania 16802, United States;* orcid.org/0000-0002-5968-3235

Complete contact information is available at: https://pubs.acs.org/10.1021/acsmaterialslett.3c00529

Author Contributions

†Y.C. and L.L. contributed equally to this work. CRediT: **Yunyun Cheng** conceptualization, formal analysis, investigation, writing-original draft; **Li Li** conceptualization, formal analysis, investigation, writing-original draft; **Caleb H. Meredith** formal analysis, investigation; **Rebecca V. Balaj** investigation; **Dingbowen Wang** investigation, resources; **Meng Pan** resources; **Ting Han** investigation; **Jian Yang** resources; **Qing Wang** resources; **Lauren D. Zarzar** project administration, resources, writing-review & editing.

Notes

The authors declare no competing financial interest.

■ ACKNOWLEDGMENTS

This work is supported by the Joint Funds of the Equipment Pre-Research of Ministry of Education of China (Grant No. 8091B022110) and the National Key R&D Program of China (Grant No. 2020YFA0711700). Y.C. acknowledges the financial support from the China Scholarship Council. L.L. thanks the National Postdoctoral Program for Innovative Talents (BX20220140) and Excellent Postdoctoral Scholarship of University for support. C.M., R.B., and L.Z. acknowledge support from the Penn State Department of Chemistry.

■ REFERENCES

(1) Banica, F.-G. *Chemical Sensors and Biosensors: Fundamentals and Applications*; John Wiley & Sons, 2012.

(2) Hammock, M. L.; Chortos, A.; Tee, B. C.-K.; Tok, J. B.-H.; Bao, Z. 25th Anniversary Article: The Evolution of Electronic Skin (E-Skin): A Brief History, Design Considerations, and Recent Progress. *Adv. Mater.* **2013**, *25* (42), 5997−6038.

(3) Blank, T. A.; Eksperiandova, L. P.; Belikov, K. N. Recent Trends of Ceramic Humidity Sensors Development: A Review. *Sens. Actuators B Chem.* **2016**, *228*, 416−442.

(4) Hua, Q.; Sun, J.; Liu, H.; Bao, R.; Yu, R.; Zhai, J.; Pan, C.; Wang, Z. L. Skin-Inspired Highly Stretchable and Conformable Matrix Networks for Multifunctional Sensing. *Nat. Commun.* **2018**, *9* (1), 244.

(5) Fratoddi, I.; Bearzotti, A.; Venditti, I.; Cametti, C.; Russo, M. V. Role of Nanostructured Polymers on the Improvement of Electrical Response-Based Relative Humidity Sensors. *Sens. Actuators B Chem.* **2016**, *225*, 96−108.

(6) Qi, Q.; Zhang, T.; Yu, Q.; Wang, R.; Zeng, Y.; Liu, L.; Yang, H. Properties of Humidity Sensing ZnO Nanorods-Base Sensor Fabricated by Screen-Printing. *Sens. Actuators B Chem.* **2008**, *133* (2), 638−643.

(7) Qiu, Y.; Yang, S. ZnO Nanotetrapods: Controlled Vapor-Phase Synthesis and Application for Humidity Sensing. *Adv. Funct. Mater.* **2007**, *17* (8), 1345−1352.

(8) Hu, X.; Gong, J.; Zhang, L.; Yu, J. C. Continuous Size Tuning of Monodisperse ZnO Colloidal Nanocrystal Clusters by a Microwave-Polyol Process and Their Application for Humidity Sensing. *Adv. Mater.* **2008**, *20* (24), 4845−4850.

(9) Chen, Q.; Nie, M.; Guo, Y. Controlled Synthesis and Humidity Sensing Properties of CdS/Polyaniline Composite Based on CdAl Layered Double Hydroxide. *Sens. Actuators B Chem.* **2018**, *254*, 30−35.

(10) Zhang, D.; Tong, J.; Xia, B. Humidity-Sensing Properties of Chemically Reduced Graphene Oxide/Polymer Nanocomposite Film Sensor Based on Layer-by-Layer Nano Self-Assembly. *Sens. Actuators B Chem.* **2014**, *197*, 66−72.

(11) Wang, S.; Xie, G.; Su, Y.; Su, L.; Zhang, Q.; Du, H.; Tai, H.; Jiang, Y. Reduced Graphene Oxide-Polyethylene Oxide Composite Films for Humidity Sensing via Quartz Crystal Microbalance. *Sens. Actuators B Chem.* **2018**, *255*, 2203−2210.

(12) Tellis, J. C.; Strulson, C. A.; Myers, M. M.; Kneas, K. A. Relative Humidity Sensors Based on an Environment-Sensitive Fluorophore in Hydrogel Films. *Anal. Chem.* **2011**, *83* (3), 928−932.

(13) Gao, R.; Yan, D.; Evans, D. G.; Duan, X. Layer-by-Layer Assembly of Long-Afterglow Self-Supporting Thin Films with Dual-Stimuli-Responsive Phosphorescence and Antiforgery Applications. *Nano Res.* **2017**, *10* (10), 3606−3617.

(14) Jung, H. S.; Verwilst, P.; Kim, W. Y.; Kim, J. S. Fluorescent and Colorimetric Sensors for the Detection of Humidity or Water Content. *Chem. Soc. Rev.* **2016**, *45* (5), 1242−1256.

(15) Kagan, C. R.; Lifshitz, E.; Sargent, E. H.; Talapin, D. V. Building Devices from Colloidal Quantum Dots. *Science* **2016**, *353* (6302), aac5523.

(16) Bae, W. K.; Char, K.; Hur, H.; Lee, S. Single-Step Synthesis of Quantum Dots with Chemical Composition Gradients. *Chem. Mater.* **2008**, *20* (2), 531−539.

(17) Meng, C.; Xiao, Y.; Wang, P.; Zhang, L.; Liu, Y.; Tong, L. Quantum-Dot-Doped Polymer Nanofibers for Optical Sensing. *Adv. Mater.* **2011**, *23* (33), 3770−3774.

(18) Xia, P.; Shou, Q.; Wang, T.; Yang, G.; Li, H.; Li, Q.; Chen, Y.; Xie, T.; Huang, J.; Xing, X. Highly Stable and Recoverable Humidity Sensor Using Fluorescent Quantum Dot Film. *Opt. Lett.* **2022**, *47* (11), 2674−2677.

(19) Cheng, Y.; Wang, H.; Li, L.; Han, T.; Liang, X.; Dong, L. Flexible Photoluminescent Humidity Sensing Material Based on Electrospun PVA Nanofibers Comprising Surface-Carboxylated QDs. *Sens. Actuators B Chem.* **2019**, *284*, 258−264.

(20) Liang, X.; Yuan, Y.; Han, T.; Cheng, Y.; Xiong, C.; Dong, L. Encapsulation and Solubilization of Ultrastable Quantum Dots with Multidentate Bilayer Ligands and Rheological Behaviour. *Nanoscale* **2018**, *10* (44), 20796−20803.

(21) Kumar, S. K.; Benicewicz, B. C.; Vaia, R. A.; Winey, K. I. 50th Anniversary Perspective: Are Polymer Nanocomposites Practical for Applications? *Macromolecules* **2017**, *50* (3), 714−731.

(22) Feng, Q.; Dong, L.; Huang, J.; Li, Q.; Fan, Y.; Xiong, J.; Xiong, C. Fluxible Monodisperse Quantum Dots with Efficient Luminescence. *Angew. Chem., Int. Ed.* **2010**, *49* (51), 9943−9946.

(23) Li, L.; Cheng, J.; Cheng, Y.; Han, T.; Liang, X.; Zhao, Y.; Zhao, G.; Dong, L. Polymer Dielectrics Exhibiting an Anomalously Improved Dielectric Constant Simultaneously Achieved High Energy Density and Efficiency Enabled by CdSe/Cd1−xZnxS Quantum Dots. *J. Mater. Chem. A* **2020**, *8* (27), 13659−13670.

(24) Hyon, S.-H.; Cha, W.-I.; Ikada, Y. Preparation of Transparent Poly(Vinyl Alcohol) Hydrogel. *Polym. Bull.* **1989**, *22* (2), 119−122.

(25) Birrer, S.; Cheon, S. I.; Zarzar, L. D. We the Droplets: A Constitutional Approach to Active and Self-Propelled Emulsions. *Curr. Opin. Colloid Interface Sci.* **2022**, *61*, 101623.

(26) Li, L.; Cheng, J.; Cheng, Y.; Han, T.; Liu, Y.; Zhou, Y.; Zhao, G.; Zhao, Y.; Xiong, C.; Dong, L.; et al. Significant Improvements in Dielectric Constant and Energy Density of Ferroelectric Polymer Nanocomposites Enabled by Ultralow Contents of Nanofillers. *Adv. Mater.* **2021**, *33* (35), 2102392.

(27) Ertuğ, B. Electrical Conductivity and Hysteresis Characteristic of BaTiO 3-Based Sensors with Polymethyl Metacry Late (PMMA) Pore Former. *Sens. Mater.* **2013**, *25* (5), 309−321.
(28) Arularasu, M. V.; Harb, M.; Vignesh, R.; Rajendran, T. V.; Sundaram, R. PVDF/ZnO Hybrid Nanocomposite Applied as a Resistive Humidity Sensor. *Surf. Interfaces* **2020**, *21*, 100780.
(29) Mallick, S.; Ahmad, Z.; Eribi, A.; Parangusan, H.; Bhadra, J.; Hassan, M. K.; Al-Thani, N. J.; Touati, F.; Al-Muhtaseb, S. Effect of Sulfonated Poly (Ether Ether Ketone) on the Sensitivity of Polyvinylidene Fluoride-Based Resistive Humidity Sensors. *Mater. Today Commun.* **2020**, *25*, 101601.
(30) Phan, D.-T.; Park, I.; Park, A.-R.; Park, C.-M.; Jeon, K.-J. Black P/Graphene Hybrid: A Fast Response Humidity Sensor with Good Reversibility and Stability. *Sci. Rep.* **2017**, *7* (1), 10561.
(31) Wang, J.; Xu, B. K.; Ruan, S. P.; Wang, S. P. Preparation and Electrical Properties of Humidity Sensing Films of BaTiO3/Polystrene Sulfonic Sodium. *Mater. Chem. Phys.* **2003**, *78* (3), 746−750.
(32) Qiang, T.; Wang, C.; Liu, M.-Q.; Adhikari, K. K.; Liang, J.-G.; Wang, L.; Li, Y.; Wu, Y.-M.; Yang, G.-H.; Meng, F.-Y.; et al. High-Performance Porous MIM-Type Capacitive Humidity Sensor Realized via Inductive Coupled Plasma and Reactive-Ion Etching. *Sens. Actuators B Chem.* **2018**, *258*, 704−714.
(33) Fernández-Ramos, M. D.; Ordóñez, Y. F.; Capitán-Vallvey, L. F.; Vargas-Sansalvador, I. M. P. de; Ballesta-Claver, J. Optical Humidity Sensor Using Methylene Blue Immobilized on a Hydrophilic Polymer. *Sens. Actuators B Chem.* **2015**, *220*, 528−533.
(34) Zhang, W.; Chen, L.; Yang, Z.; Peng, J. An Optical Humidity Sensor Based on Li3PO4 Hollow Nanospheres. *Sens. Actuators B Chem.* **2011**, *155* (1), 226−231.
(35) Hu, J.; Wu, P.; Deng, D.; Jiang, X.; Hou, X.; Lv, Y. An Optical Humidity Sensor Based on CdTe Nanocrystals Modified Porous Silicon. *Microchem. J.* **2013**, *108*, 100−105.
(36) Larkin, P. *Infrared and Raman Spectroscopy: Principles and Spectral Interpretation*; Elsevier, 2017.
(37) Frisch, M.; Trucks, G. W.; Schlegel, H. B.; Scuseria, G. E.; Robb, M. A.; Cheeseman, J. R.; Scalmani, G.; Barone, V.; Mennucci, B.; Petersson, G.; et al. *Gaussian 09, Revision D.01*; Gaussian, Inc.: Wallingford CT, 2009.
(38) Lu, T.; Chen, F. Multiwfn: A Multifunctional Wavefunction Analyzer. *J. Comput. Chem.* **2012**, *33* (5), 580−592.
(39) Lu, T.; Chen, Q. Independent Gradient Model Based on Hirshfeld Partition: A New Method for Visual Study of Interactions in Chemical Systems. *J. Comput. Chem.* **2022**, *43* (8), 539−555.
(40) Chen, J.; Hurtubise, R. J. Infrared Study of the Interactions of Moisture with Filter Paper and the Moisture Quenching of Solid-Matrix Room Temperature Phosphorescence. *Anal. Chim. Acta* **1996**, *324* (1), 61−68.
(41) Zhao, Y.; Riemersma, C.; Pietra, F.; Koole, R.; de Mello Donegá, C.; Meijerink, A. High-Temperature Luminescence Quenching of Colloidal Quantum Dots. *ACS Nano* **2012**, *6* (10), 9058−9067.
(42) Sung Jung, H.; Verwilst, P.; Young Kim, W.; Seung Kim, J. Fluorescent and Colorimetric Sensors for the Detection of Humidity or Water Content. *Chem. Soc. Rev.* **2016**, *45* (5), 1242−1256.
(43) Jin, W. J.; Costa-Fernández, J. M.; Pereiro, R.; Sanz-Medel, A. Surface-Modified CdSe Quantum Dots as Luminescent Probes for Cyanide Determination. *Anal. Chim. Acta* **2004**, *522* (1), 1−8.
(44) Hua, M.; Wu, S.; Ma, Y.; Zhao, Y.; Chen, Z.; Frenkel, I.; Strzalka, J.; Zhou, H.; Zhu, X.; He, X. Strong Tough Hydrogels via the Synergy of Freeze-Casting and Salting Out. *Nature* **2021**, *590* (7847), 594−599.
(45) Wang, Z.; Zheng, X.; Ouchi, T.; Kouznetsova, T. B.; Beech, H. K.; Av-Ron, S.; Matsuda, T.; Bowser, B. H.; Wang, S.; Johnson, J. A.; et al. Toughening Hydrogels through Force-Triggered Chemical Reactions That Lengthen Polymer Strands. *Science* **2021**, *374* (6564), 193−196.
(46) Wu, S.; Hua, M.; Alsaid, Y.; Du, Y.; Ma, Y.; Zhao, Y.; Lo, C.-Y.; Wang, C.; Wu, D.; Yao, B.; et al. Poly(Vinyl Alcohol) Hydrogels with Broad-Range Tunable Mechanical Properties via the Hofmeister Effect. *Adv. Mater.* **2021**, *33* (11), 2007829.
(47) Lee, S.; Hamonangan, W. M.; Kim, J. H.; Kim, S.-H. Soft and Tough Microcapsules with Double-Network Hydrogel Shells. *Adv. Funct. Mater.* **2022**, *32* (34), 2203761.
(48) Wang, T.; Zhang, Y.; Liu, Q.; Cheng, W.; Wang, X.; Pan, L.; Xu, B.; Xu, H. A Self-Healable, Highly Stretchable, and Solution Processable Conductive Polymer Composite for Ultrasensitive Strain and Pressure Sensing. *Adv. Funct. Mater.* **2018**, *28* (7), 1705551.
(49) Li, H.; Yang, T.; Zhou, Y.; Ai, D.; Yao, B.; Liu, Y.; Li, L.; Chen, L.-Q.; Wang, Q. Enabling High-Energy-Density High-Efficiency Ferroelectric Polymer Nanocomposites with Rationally Designed Nanofillers. *Adv. Funct. Mater.* **2021**, *31* (1), 2006739.
(50) Li, L.; Feng, R.; Zhang, Y.; Dong, L. Flexible, Transparent and High Dielectric-Constant Fluoropolymer-Based Nanocomposites with a Fluoride-Constructed Interfacial Structure. *J. Mater. Chem. C* **2017**, *5* (44), 11403−11410.
(51) Kim, J. W.; Park, H.; Lee, G.; Jeong, Y. R.; Hong, S. Y.; Keum, K.; Yoon, J.; Kim, M. S.; Ha, J. S. Paper-Like, Thin, Foldable, and Self-Healable Electronics Based on PVA/CNC Nanocomposite Film. *Adv. Funct. Mater.* **2019**, *29* (50), 1905968.
(52) Guo, Y.; Zheng, K.; Wan, P. A Flexible Stretchable Hydrogel Electrolyte for Healable All-in-One Configured Supercapacitors. *Small* **2018**, *14* (14), 1704497.

https://doi.org/10.1021/acsmaterialslett.3c00529
ACS Materials Lett. 2023, 5, 2074−2083